

Subunit Orientation in the *Escherichia coli* Enterobactin Biosynthetic EntA-EntE Complex Revealed by a Two-Hybrid Approach

Paknoosh Pakarian[¶], and Peter D. Pawelek^{¶♦*}

[¶] Department of Chemistry and Biochemistry, Concordia University, 7141 Sherbrooke St., W., Montreal, Quebec, Canada, H4B 1R6

♦Groupe de Recherche Axé sur la Structure des Protéines (GRASP)

*Correspondence should be addressed to: Peter D. Pawelek, Tel: 514-848-2424 ext. 3118; Fax: 514-848-2868; E-mail: peter.pawelek@concordia.ca.

Running title: "Subunit orientation in the intracellular EntA-EntE complex"

Supplementary material: None

ABSTRACT

The siderophore enterobactin is synthesized by the enzymes EntA-F and EntH in the *E. coli* cytoplasm. We previously reported *in vitro* evidence of an interaction between tetrameric EntA and monomeric EntE. Here we used bacterial adenylate cyclase two-hybrid (BACTH) assays to demonstrate that the *E. coli* EntA-EntE interaction occurs intracellularly. Furthermore, to obtain information on subunit orientation in the EntA-EntE complex, we fused BACTH reporter fragments T18 and T25 to EntA and EntE in both N-terminal and C-terminal orientations. To validate functionality of our fusion proteins, we performed Chrome Azurol S (CAS) assays using *E. coli entE*⁻ and *entA*⁻ knockout strains transformed with our BACTH constructs. We found that transformants expressing N-terminal and C-terminal T18/T25 fusions to EntE exhibited CAS signals, indicating that these constructs could rescue the *entE*⁻ phenotype. While expression of EntA with N-terminal T18/T25 fusions exhibited CAS signals, C-terminal fusions did not, presumably due to disruption of the EntA tetramer *in vivo*. Bacterial growth assays supported our CAS findings. Co-transformation of functional T18/T25 fusions into *cya*⁻ *E. coli* BTH101 cells resulted in positive BACTH signals only when T18/T25 fragments were fused to the N-termini of both EntA and EntE. Co-expression of N-terminally fused EntA with C-terminally fused EntE resulted in no detectable BACTH signal. Analysis of protein expression by Western blotting confirmed that the loss of BACTH signal was not due to impaired expression of fusion proteins. Based on our results, we propose that the N-termini of EntA and EntE are proximal in the intracellular complex, while the EntA N-terminus and EntE C-terminus are distal. A protein-protein docking simulation using SwarmDock was in agreement with our experimental observations.

Keywords: siderophore; enterobactin; protein-protein interactions; bacterial two-hybrid; CAS assay.

Abbreviations: BACTH: bacterial adenylate cyclase two-hybrid; CAS: chrome azurol S; DHB: 2,3-dihydroxybenzoic acid; DTT: dithiothreitol; Fur: Ferric Uptake Regulator; HRP: horseradish peroxidase; IPTG: isopropyl β -D-1-thiogalactopyranoside; NRPS: non-ribosomal peptide synthesis; PVDF: polyvinylidene difluoride; SDS-PAGE: SDS-polyacrylamide gel electrophoresis.

1. Introduction

The Gram-negative bacterium *Escherichia coli* employs siderophore-mediated iron acquisition as a dominant means of importing extracellular iron under conditions of iron starvation [1]. The two major siderophores of *E. coli* are the hydroxamate siderophore aerobactin and the catecholate siderophore enterobactin [2,3]. Enterobactin consists of three dihydroxybenzoate groups linked by a triserine lactone core. It is synthesized in the *E. coli* cytoplasm and then secreted in the *apo* form to chelate extracellular Fe^{3+} . Uptake of ferric enterobactin is then mediated by a TonB-dependent uptake system [4]. Biosynthesis of enterobactin occurs in a pathway containing two major functional arms: (1) synthesis of 2,3-dihydroxybenzoic acid (DHB) from chorismate as catalyzed by the sequentially-related enzymes EntC, EntB (N-terminal isochorismatase domain), and EntA; (2) condensation of three molecules of DHB with three molecules of L-serine *via* a non-ribosomal peptide synthesis (NRPS) 'assembly line' comprised of the enzymes EntE, EntB (C-terminal aryl carrier protein domain), EntD, and EntF [5]. The thioesterase EntH has been shown to play a proofreading role in enterobactin biosynthesis [6]. Expression of the genes encoding the enterobactin biosynthetic enzymes (*entA-F, H*) is up-regulated during conditions of low intracellular iron, due to de-repression by the Ferric Uptake Regulator (Fur) protein.

Obligate protein-protein interactions in the NRPS arm have been known for many years [7-11]. In addition, we have previously reported *in vitro* evidence of an interaction between EntA, the terminal enzyme in the DHB synthetic arm of the pathway, and EntE, the initial enzyme in the NRPS arm of the pathway [12]. The existence of an EntA-EntE interaction, in addition to those within the NRPS module, is consistent with recent reports of membrane-associated "siderosomes" in *Pseudomonas aeruginosa* that are involved in pyoverdine and pyochelin

biosynthesis [13,14]. We found that the EntA-EntE interaction stimulated EntE activity approximately 4-fold, presumably by inducing conformational alterations at the EntE active site. Furthermore, biophysical approaches revealed that the affinity of the EntA-EntE interaction increased when EntA was in the tetrameric form relative to the dimeric form [12]. Here we demonstrate intracellular EntA-EntE complex formation in *E. coli* using a bacterial adenylate cyclase two-hybrid (BACTH) approach. BACTH constructs were functionally validated by Chrome Azurol S (CAS) assays and growth studies. Our BACTH assays revealed relative orientations of EntA and EntE subunits within the intracellular complex. Automated docking simulations supported our BACTH observations.

2. Materials and Methods

2.1 Reagents

All chemicals were purchased from Bioshop Canada, Inc. (Burlington, Ontario) unless noted otherwise.

2.2 Preparation of BACTH constructs

Genes encoding *E. coli* EntA and EntE were PCR-amplified from pCA24N-*entA* and pCA24N-*entE* vectors, respectively, obtained from the ASKA collection [15]. PCR primers (Table 1) were designed such that *KpnI* and *EcoRI* sites were incorporated flanking the open reading frames. Amplification was performed using Phusion High-Fidelity DNA polymerase (New England Biolabs) according to the manufacturer's standard protocol. For recombinant BACTH fusion protein expression, PCR-amplified *entA* and *entE* genes were subcloned in-frame between *KpnI* and *EcoRI* sites of pUT18C and pKT25 (Euromedex) such that fragments of the catalytic domain of *B. pertussis* adenylate cyclase (T18 and T25) were fused N-terminally to

EntA and EntE with vector-encoded polypeptide linker sequences N-HCRSTLEDPRVP-C (T18) and N-AAGSTLEDPRVP-C (T25) between EntA/EntE and T18/T25 fragments. For C-terminal T18/T25 fusions, PCR-amplified *entA* and *entE* genes were similarly subcloned into pUT18 and pKNT25 (Euromedex). Although the BACTH vectors with N-terminal T18/T25 fusions encoded 12-residue linkers, the linker between the EcoRI site and the DNA encoding C-terminal T18 and T25 fusions in the pUT18 and pKNT25 vectors had a length of only nine nucleotides encoding three residues. For subcloning our genes into these vectors, we used primers encoding an additional 9-residue HA tag linker (N-YPYDVPDYA-C) (Table 1). PCR products encoding EntA/EntE-HA fusions were subcloned between *KpnI* and *EcoRI* sites of pUT18 and pKNT25 vectors such that T18 and T25 fragments were fused C-terminally to EntA/EntE-HA upon induction of protein expression. All constructs were verified by DNA sequencing (Genome Quebec Innovation Centre, McGill University).

2.3 Modification of *entA*⁻ and *entE*⁻ knockout strains

BACTH constructs containing *entA* or *entE* genes were individually transformed into respective *entA*⁻ or *entE*⁻ single knockout strains to determine if the plasmid-borne *entA/entE* gene products fused to T25 or T18 could rescue the knockout phenotypes. We used modified *E. coli* BW25113 (F⁻, Δ (*araD-araB*)567, Δ *lacZ*4787(*::rrnB-3*), λ ⁻, *rph-1*, Δ (*rhaD-rhaB*)568, *hsdR514*) [16] strains obtained from the KEIO collection [17] that had *entA* or *entE* genes disrupted by insertion of a kanamycin resistance cassette. Since the T25-encoding BACTH constructs contained a kanamycin resistance gene (*kanR*) as a selective marker, we removed the chromosomally-inserted *kanR* genes from the KEIO strains by using the Wanner Lambda Red Gene disruption kit (The Coli Genetic Stock Center (Yale CGSC)) [16]. Briefly, pCP20 plasmid

was used for temperature-sensitive removal of *kanR* genes flanked by FRT (FLP Recognition Target) sequences. Competent knockout strains were transformed with pCP20 and were incubated overnight at 30 °C on LB plates containing 100 µg ml⁻¹ ampicillin. Colony picks were streaked on LB plates (no antibiotic) and incubated at 43 °C overnight. The loss of chromosomal *kanR* antibiotic resistance gene and pCP20 plasmid was verified by re-streaking colonies onto LB agar containing 50 µg ml⁻¹ kanamycin and 100 µg ml⁻¹ ampicillin, respectively.

2.4 CAS assays and growth studies

Competent modified knockout background strains (*kanR*⁻ *entA*⁻ or *kanR*⁻ *entE*⁻) were transformed with respective BACTH constructs. Strains transformed with pKT25 or pKNT25 constructs were plated on LB agar containing 50 µg ml⁻¹ kanamycin, whereas strains transformed with pUT18C or pUT18 constructs were selected on LB plates supplemented with 100 µg ml⁻¹ ampicillin. Strains transformed with pCA24N-derived constructs were plated on LB agar containing 34 µg ml⁻¹ chloramphenicol. Empty vectors were also transformed into *entA*⁻ and *entE*⁻ modified knockout background strains as controls. All plates were incubated overnight at 30 °C. Colonies from transformation plates were used to inoculate LB broth supplemented with 50 µg ml⁻¹ kanamycin or 100 µg ml⁻¹ ampicillin or 34 µg ml⁻¹ chloramphenicol as appropriate. The cultures were incubated with shaking at 30 °C. Overnight cultures were diluted 1:100 in LB broth supplemented with 50 µg ml⁻¹ kanamycin or 100 µg ml⁻¹ ampicillin or 34 µg ml⁻¹ chloramphenicol and grown at 30 °C until an OD₆₀₀ between 0.5 – 0.7 was observed. Cultures were then diluted 1:1,000 in M9 medium composed of 1X M9 salts [18] supplemented with 0.3% (w/v) casamino acids, 0.2% (w/v) D-glucose, 1 mM MgCl₂, 100 µM CaCl₂, 0.0002% (w/v) thiamine HCl, 0.5 mM IPTG and 50 µg ml⁻¹ kanamycin or 100 µg ml⁻¹ ampicillin or 34 µg ml⁻¹

chloramphenicol. Cultures diluted in minimal medium were grown at 30 °C overnight. CAS-agar plates were prepared according to Payne *et al.* [19] and then spotted with 1 µL overnight cultures in M9 medium and incubated at 30 °C for 16 to 20 hours. The CAS signal was interpreted as the presence of an orange halo, indicative of enterobactin biosynthesis [20]. Each CAS assay was performed at least in triplicate to ensure reproducibility.

For bacterial growth studies, single colony picks of *E. coli* cells (wild-type and knockout strains +/- transformed plasmids) were used to inoculate cultures as described above. Cultures were grown at 30 °C until they reached an OD₆₀₀ of 1.00, and then centrifuged for 1 min at 21,000 x g and cell pellets were resuspended in 1X M9 medium. All cell suspensions were adjusted to a final OD₆₀₀ of 1.00. Bacterial suspensions were then diluted 1:1,000 in 1X M9 medium with 0.5 mM IPTG, appropriate antibiotics (see above), and 50 µM 2,2'-dipyridyl followed by incubation at 30 °C for 18 hours with shaking. After incubation, the OD₆₀₀ of all cultures were measured. Growth experiments were performed in triplicate for each transformant/strain.

2.5 Bacterial adenylate cyclase two-hybrid (BACTH) assays

BACTH constructs that could rescue *entA*⁻ or *entE*⁻ knockout phenotypes were co-transformed into competent *E. coli* BTH101 cells (F⁻, *cya-99*, *araD139*, *galE15*, *galk16*, *rpsL1* (*Str*^R), *hsdR2*, *mcrA1*, *mcrB1*) (Euromedex). Co-transformants were incubated on LB plates containing 100 µg ml⁻¹ ampicillin and 50 µg ml⁻¹ kanamycin at 30 °C for two days. Colony picks were used to inoculate 3 ml of LB medium containing 100 µg ml⁻¹ ampicillin, 50 µg ml⁻¹ kanamycin and 0.5 mM IPTG. Inoculated cultures were grown at 30 °C overnight [21]. β-galactosidase assays of overnight cultures were performed in triplicate as described by Miller

[22] except that reactions were incubated at room temperature. For plate assays, 1 μl of each overnight culture was spotted onto MacConkey agar base (Difco) plates containing 100 $\mu\text{g ml}^{-1}$ ampicillin, 50 $\mu\text{g ml}^{-1}$ kanamycin, 0.5 mM IPTG and 1% maltose. Spotted plates were incubated at 30 °C for 18-24 hours [21]. Plate assays were also performed at least in triplicate with reproducible results. BACTH signals (i.e., interaction of fusion gene products in co-transformants) were interpreted as the formation of red colonies on MacConkey agar plates [23], and by elevated Miller units (at least 5-fold) relative to appropriate controls in β -galactosidase assays.

2.6 Western blotting

BACTH expression constructs encoding EntA/EntE-T18/T25 fusions were transformed into competent *E. coli* BW25113. One colony of each transformant was used to inoculate 2 ml of LB broth containing 100 $\mu\text{g ml}^{-1}$ ampicillin or 50 $\mu\text{g ml}^{-1}$ kanamycin. Cultures were incubated at 30° C overnight with agitation. Overnight cultures were diluted 1:100 in 5 ml LB broth containing 100 $\mu\text{g ml}^{-1}$ ampicillin or 50 $\mu\text{g ml}^{-1}$ kanamycin and were incubated at 30° C with shaking until an OD_{600} between 0.5-0.7 was reached. IPTG was then added to a final concentration of 0.5 mM, and induced cultures were grown at 30° C for an additional 16 h. Cells (100 mg wet weight) from overnight cultures were pelleted by centrifugation at 3,000 x g at 4° C for 30 minutes and then resuspended in lysis buffer (50mM Tris pH8, 1% n-octyl-B-D-thioglucopyranoside, 3 $\mu\text{g/ml}$ DNase, 3 $\mu\text{g/ml}$ RNaseI, 30 $\mu\text{g/ml}$ lysozyme, 1mM DTT, 1X Proteinase Inhibitor Cocktail) and incubated on a nutating mixer for 30 minutes at room temperature. Aliquots of total cell lysates were separated on 8% SDS-polyacrylamide gels. Lysates from untransformed *E. coli* BW25113 cells were used as negative controls. Following

gel electrophoresis, separated proteins were transferred onto a PVDF membrane using a Mini-Trans Blot Electrophoretic Transfer Cell (Bio-Rad Laboratories). Membranes were blocked using 5% skim milk powder in PBST (137 mM NaCl, 2.7 mM KCl, 10 mM Na₂HPO₄, 1.8 mM KH₂PO₄, 0.2% Tween 20) for 1h at room temperature. Blocked membranes were incubated with one of the following primary antibodies for 1h at room temperature: (i) mouse monoclonal anti-Cya A (3D1) antibody (1:10,000 dilution, Santa Cruz Biotechnology) that recognizes the T18 fragment, (ii) goat polyclonal anti-Cya A (bN-13) (1:1,000 dilution, Santa Cruz Biotechnology) that recognizes the T25 fragment, or (iii) mouse monoclonal anti-HA antibody (1:5,000, Thermo Fisher Scientific) that recognizes the HA tag linker incorporated into our C-terminally tagged BACTH constructs. Goat anti-mouse conjugated with horseradish peroxidase (HRP) (1:15,000 - 1:10,000 dilution, Santa Cruz Biotechnology) and donkey anti-goat conjugated with HRP (1:5,000 dilution, Santa Cruz Biotechnology) were used as secondary antibodies. HRP activity was visualized using a SuperSignal™ West Pico Chemiluminescent Substrate (Thermo Fisher Scientific).

2.7 Automated Docking

Atomic coordinates of EntE monomer and EntA tetramer X-ray crystallographic structures were submitted to the SwarmDock server [24] for a blind docking experiment. The submitted EntE ligand consisted of residues 2-536 from the structure of the tethered EntB-EntE chimera (PDB code: 3RG2) reported previously [25]. The submitted receptor was the EntA tetramer (PDB code: 2FWM, biological assembly (chains A-D)) [26]. All SwarmDock parameters were left as default (number of normal modes: 5, docking type: full blind).

3. Results and Discussion

Our laboratory previously demonstrated that *E. coli* EntA and EntE form a complex *in vitro* [12]. Furthermore, we found that this interaction has a higher affinity when EntA is in the tetrameric state. Here we employed the bacterial adenylate cyclase two-hybrid (BACTH) system to study the intracellular interaction between EntA and EntE, and to gain further insights into the role of EntA oligomerization in EntA-EntE complex assembly. BACTH has previously been used to identify intracellular interactions between the thioesterase EntH and the ArCP domain of EntB [6]. In this study, we employed BACTH to investigate an interaction between enterobactin biosynthetic enzymes at the functional hinge between DHB biosynthesis and downstream NRPS processes. We prepared combinatorial BACTH constructs that encoded EntA and EntE with N- and C-terminal fusions to fragments (T18 and T25) of the catalytic domain of *B. pertussis* adenylate cyclase [23].

3.1 Validation of BACTH constructs using CAS assays and growth studies

Prior to using our T18/T25 fusion constructs in BACTH assays, we performed validation experiments to investigate whether constructs encoding our T18/T25-EntA/EntE fusion proteins were functional in respective *entA*⁻ or *entE*⁻ backgrounds. Given that addition of polypeptide tags may potentially alter protein activity [27], we wanted to ensure that intracellular enzymatic functions of BACTH fusion proteins were not impaired by the N- or C-terminal addition of adenylate cyclase fragments T18 and T25. BACTH constructs were transformed into competent *E. coli entA*⁻ or *entE*⁻ knockout cells, and CAS agar assays were performed to determine if transformants produced orange halos indicative of enterobactin biosynthesis [20]. The presence of halos indicated that the T18/T25-fusion protein could rescue the knockout phenotype, thus

confirming retention of Ent protein functionality. Fig. 1A shows CAS assay outcomes of the untransformed *E. coli* control strains: wild-type BW25113 (Fig. 1A: wt), BW25113 *entA*⁻ (Fig. 1A: *entA*⁻), and BW25113 *entE*⁻ (Fig. 1A: *entE*⁻). As expected, wild-type BW25113 cells produced an orange halo indicative of enterobactin biosynthesis, whereas the *entA*⁻ and *entE*⁻ knockout strains exhibited no halo due to impaired enterobactin production. Growth studies on untransformed strains indicated that wild-type BW25113 cells (Fig. 1A, bar graph 1) exhibited the highest cell density in comparison to BW25113 *entA*⁻ and *entE*⁻ strains, which grew poorly in iron-deprived medium (Fig. 1A, bar graph 2 & 3). To ensure that observed CAS signals were independent of the nature of the polypeptide sequences fused to EntA or EntE, we performed control assays in which *E. coli* BW25113 cells were transformed with pCA24N-based expression constructs encoding EntA and EntE with N-terminal hexahistidine tags. We previously used these constructs to express and purify functional H6-EntA and H6-EntE [12]. Transformation of pCA24N-H6-*entA* into an *entA*⁻ background was found to successfully rescue the knockout phenotype resulting in a CAS halo (Fig. 1B, upper panel) and resulted in elevated growth relative to *entA*⁻ cells transformed with empty pCA24N vector (Fig. 1B, bar graph 1 & 2). Similar results were found for BW25113 cells transformed with pCA24N-H6-*entE* into an *entE*⁻ background (Fig. 1B, lower panel; Fig. 1B, bar graph 3 & 4).

We then assessed the functionality of our BACTH constructs. BW25113 *entA*⁻ cells transformed with pKT25-*entA* (Fig. 1C upper panel: T25-EntA) produced an orange halo, indicating that recombinant EntA with T25 fused to the N-terminus did not disrupt intracellular EntA function. However, cells transformed with pKNT25-*entA* (Fig. 1C upper panel: EntA-T25), which expressed recombinant EntA with T25 fused to the C-terminus, did not produce a halo. Consistent with our CAS assays, growth studies showed that only N-terminally tagged T25-EntA

could complement the knockout phenotype, whereas C-terminally tagged EntA-T25 grew as poorly as the empty vector control (Fig. 1C, upper bar graph: 1-4). This demonstrates that EntA with C-terminally fused T25 fragment could not rescue the *entA*⁻ phenotype. Similar results were found for fusion of T18 to EntA, where fusion of T18 to the N-terminus of EntA rescued the knockout phenotype (Fig. 1C, lower panel: T18-EntA), but not fusion of T18 to the EntA C-terminus (Fig. 1C, lower panel: EntA-T18). Growth studies on transformants expressing T18-EntA and EntA-T18 also indicated that only T18-EntA could complement the *entA*⁻ knockout phenotype, whereas transformants expressing EntA-T18 did not exhibit higher growth than the vector control (Fig. 1C, lower bar graph: 1-4). The functional assessment of *entE*-harboring BACTH constructs is shown in Figure 1D. Here, transformants expressing T25-fused EntE produced orange halos whether T25 was fused N- or C-terminally (Fig. 1D, upper panel: T25-EntE, EntE-T25). Transformants expressing T25-EntE or EntE-T25 exhibited higher growth in comparison with vector control transformants, indicating the ability of these fusion proteins to rescue the *entE*⁻ knockout phenotype (Fig. 1D, upper bar graph: 1-4). Fusion of the T18 fragment to EntE also resulted in functional constructs independent of the position of T18 relative to EntE (Fig. 1D, lower panel: T18-EntE, EntE-T18), although T18-EntE exhibited a more intense halo than EntE-T18. Growth studies demonstrated that transformants expressing either T18-EntE or EntE-T18 could rescue the *entE*⁻ knockout phenotype relative to vector controls (Fig. 1D, lower bar graph: 1-4). For both *entA*⁻ and *entE*⁻ knockout strains, no CAS halos were observed when cells were transformed with empty BACTH vectors (Figs. 1C and 1D, upper and lower panels: T25-vec, vec-T25, T18-vec, vec-T18). Since the *entA* and *entE* genes occur in an operon (*entCEBAH*) in the *E. coli* chromosome [6], possible loss of functionality in single-gene knockouts may be due to polar effects on downstream genes in the operon. However, Datsenko

and Wanner (2000) [16] demonstrated that their single-gene disruptions in *E. coli* BW25113 had no polar effects on downstream gene expression. Consistent with this, we found that complementation of our *entE*⁻ knockout strain with *in trans* expression of T18- or T25-fused EntE resulted in positive CAS signals, demonstrating functionality of downstream *entB*, *entA*, and *entH* genes in the operon in an *entE*⁻ background.

Our CAS assay and growth study outcomes are summarized in Table 2. We found that T18-EntA and T25-EntA were able to complement the *entA*⁻ phenotype as seen in our CAS assays (Table 2, column 4, rows 1 and 3). However, EntA-T18 and EntA-T25 could not rescue the *entA*⁻ phenotype, suggesting a disruption of EntA intracellular function (Table 2, column 4, rows 2 and 4). The X-ray crystallographic structure of tetrameric EntA (PDB code: 2FWM) [26] revealed that the C-terminus of each monomeric subunit projects towards the interior of the tetramer, whereas the N-termini extend away from the protein (Fig. 2A). The introduction of T18 and T25 fusions to EntA C-termini may therefore prevent formation of EntA tetramers *in vivo*, thus negatively affecting enterobactin biosynthesis. In contrast, all EntE fusions examined (T18-EntE, T25-EntE, EntE-T18, EntE-T25) could rescue the *entE*⁻ phenotype, demonstrating that these fusions did not disrupt the intracellular function of EntE (Table 2, column 5, rows 1-4). Inspection of the published X-ray crystallographic structure of monomeric EntE (PDB code: 3RG2) [25], which was expressed as a tethered EntE-EntB fusion, indicates that the N- and C-termini both project away from the center of protein mass (Fig. 2B), consistent with our observation that both N-terminal and C-terminal EntE fusions were functionally active. These findings were useful in guiding us in the selection of BACTH constructs to use in our bacterial two-hybrid assays. Since pKT25-*entA* and pUT18C-*entA* could complement the *entA*⁻ phenotype, we proceeded with using them for BACTH since we were confident that the EntA portions of

expressed N-terminal EntA fusions were functional. The pKNT25-*entA* and pUT18-*entA* constructs were rejected for BACTH due to their lack of functionality. We proceeded to use all *entE* BACTH constructs for our two-hybrid studies since they were all found to be functional *via* CAS assays and growth studies.

3.2 Detection of the intracellular EntA-EntE interaction by BACTH

BACTH constructs were co-transformed into *E. coli* BTH101 cells. Colonies of co-transformants grown on LB-agar plates were picked and cultured overnight in LB medium. Aliquots (1 μ l) of overnight cultures were spotted onto MacConkey agar plates followed by incubation at 30 °C for 18-24 hours [21]. The co-transformant expressing T25-EntA and T18-EntE demonstrated a positive BACTH signal (Fig. 3A, column 1). Similar results were seen in the co-transformant expressing T18-EntA and T25-EntE (Fig. 3A, column 2). However, the co-transformant expressing T18-EntA and EntE-T25 did not result in a BACTH signal (Fig. 3A, column 3). This was also observed for the co-transformant expressing T25-EntA and EntE-T18 (Fig. 3A, column 4). Taken together, BACTH signals were only observed when T18/T25 fusions were located at the N-termini of both EntA and EntE. β -galactosidase assay results for the complete set of co-transformants that we investigated in this study are shown in Fig. 3B. Consistent with our MacConkey agar plate assays, EntA and EntE co-transformants containing N-terminal T18/T25 fusions produced the highest levels of β -galactosidase activity (363 ± 38 Miller units and 308 ± 14 Miller units, respectively), confirming that the EntA-EntE interaction was only observed with N-terminally fused EntA and EntE (Fig. 3B, columns 1 and 2). We observed a lack of BACTH signal for co-transformants in which N-terminal T18/T25-EntA fusions were co-expressed with C-terminal EntE-T25/T18 fusions (Fig. 3B, columns 3 and 4).

The positive BACTH signals seen for N-terminally fused EntA and EntE co-transformants were significantly higher than all negative controls in which BTH101 cells were co-transformed with empty vectors (Fig. 3B, columns 5-11). An additional control was performed in which pKT25-*entA* was co-transformed with a BACTH construct expressing a protein unrelated to enterobactin biosynthesis (pUT18C-*mobA*). This co-transformant also resulted in β -galactosidase activity no higher than the vector controls (Fig. 3B, column 12). The *E. coli* protein MobA is involved in molybdenum cofactor biosynthesis, and N-terminally fused MobA BACTH constructs have previously been shown to be active [28]. In contrast, a leucine zipper positive control (BTH101 cells co-transformed with pKT25-zip and pUT18C-zip provided in Euromedex kit) yielded $4,539 \pm 222$ Miller units under identical assay conditions (not shown). The lack of BACTH signal in the T25/T18-EntA and EntE-T25/T18 co-transformants (Fig. 3B, columns 3 and 4) indicates that the EntE C-terminus is distant from EntA N-termini in the EntA-EntE complex since the BACTH signal relies on proximity of T18 and T25 fragments for reconstitution of adenylate cyclase activity. Taken together, our BACTH results provide initial evidence of the relative orientations of EntA and EntE subunits in the EntA-EntE complex upon formation of the interaction interface.

3.3 Intracellular expression of BACTH fusion proteins

In order to confirm that the lack of two-hybrid signal observed for co-transformants expressing T18-EntA/EntE-T25 and T25-EntA/EntE-T18 was not due to impaired protein expression, all eight constructs were individually transformed into *E. coli* BW25113 for protein expression studies. BACTH vectors are under the control of the *lac* promoter and require cAMP for expression [29]. It is recommended that studies of fusion protein expression from these

vectors should be performed in a *cya*⁺ strain such as BW25113 [21,30]. We therefore examined BACTH fusion protein expression in *E. coli* BW25113 whole-cell lysates following transformation of individual BACTH constructs and IPTG induction. For Western analysis of whole-cell lysates, membranes were probed with appropriate anti-T18 (3D1), anti-T25 (bN-13), and anti-HA antibodies (Fig. 4). All transformants were found to express T25/T18 fusion proteins. Furthermore, C-terminal fusion proteins containing HA tags were detected by anti-HA antibody. These results confirmed that the lack of two-hybrid signals for co-transformants containing N-terminally fused EntA and C-terminally fused EntE was not due to impaired intracellular protein expression from the BACTH constructs.

3.4 Computational prediction of the EntA-EntE complex

To gain further insights into the nature of EntA-EntE interaction revealed by our two-hybrid approach, we submitted X-ray crystallographic structures of EntA (PDB code: 2FWM) and EntE (PDB code: 3RG2) to the SwarmDock server [24], which was chosen for its ability to introduce flexibility in the automated docking operation as well as for its high-scoring performance in the CAPRI competition [32]. Full-blind docking of monomeric EntE to the EntA tetramer resulted in the highest-scoring and lowest-energy ensemble shown in Figure 5. The docked ensemble (top-ranked out of a total of 444 candidate ensembles returned by the server) was found to contain one EntE monomer interacting with one face of the EntA tetramer. Furthermore, the EntE C-terminal domain (residues 432-536), which has been proposed to undergo conformational rearrangement as part of domain alternation mechanism [8], is facing away from the EntA-EntE interaction interface (Fig. 5A). A similar blind docking job was submitted to the ClusPro server [33], which also returned its highest-scoring ensemble with the

same stoichiometry and orientation of EntE relative to the EntA tetramer (data not shown). We focus here on the SwarmDock ensemble since flexible docking algorithms are more robust in predicting atomic positions of unstructured regions such as protein termini [33]. Flexible modeling of termini positions is important in the context of BACTH in order to model exit points for T18 and T25 fusions. In the SwarmDock model, EntE residues at the interaction interface are entirely from the N-terminal portion of the protein (Fig. 5A). This orientation is consistent with the BACTH outcomes reported here in which the C-terminus of EntE is distant from EntA N-termini. In the model, the N-terminus of EntE exits the complex at a position such that when fused to T18 or T25, it could be proximal to T25 or T18 fused to the N-termini of EntA subunits C or D. A contact map generated from the predicted complex indicates that residues from all four subunits of the EntA tetramer occur at the interaction interface (Fig. 5B). This is in agreement with our CAS results suggesting that the EntA tetramer is required for biological functionality, and is consistent with our previous report of EntE being unable to interact favorably with EntA in the dimeric or monomeric forms [12]. Although SwarmDock only modeled EntE interaction at one face of the EntA tetramer, EntA possesses two symmetric solvent-exposed surfaces. The overall stoichiometry of the intracellular complex consistent with the SwarmDock model would therefore be two EntE monomers binding per EntA tetramer. This agrees with the stoichiometry value (0.79 ± 0.19) that we previously determined by isothermal titration microcalorimetry [12].

In conclusion, the experimental outcomes reported here provide initial information on the overall subunit orientation of the EntA-EntE complex as it occurs in *E. coli* cells. A blind docking simulation supports our experimental data that elucidate the orientation of EntA and EntE in the complex as well as the biological importance of the quaternary structure of EntA.

This knowledge will be useful in further exploring the EntA-EntE protein interaction interface at the functional hinge of the DHB biosynthetic and NRPS modules.

Acknowledgements

This work was supported by Discovery Grant 341983 from the Natural Sciences and Engineering Research Council of Canada to P.D.P. Financial support for P. Pakarian was provided by an FQRNT PBEEE/MELS Scholarship and GRASP. We acknowledge NBRP-*E. coli* at NIG (Japan) for providing KEIO strains.

References

1. Miethke, M. and Marahiel, M.A. (2007) Siderophore-based iron acquisition and pathogen control. *Microbiol Mol Biol Rev.* **71**: 413-451.
2. de Lorenzo, V., Bindereif, A., Paw, B.H. and Neilands, J.B. (1986) Aerobactin biosynthesis and transport genes of plasmid ColV-K30 in *Escherichia coli* K-12. *J Bacteriol.* **165**: 570-578.
3. Raymond, K.N., Dertz, E.A. and Kim, S.S. (2003) Enterobactin: an archetype for microbial iron transport. *Proc Natl Acad Sci U S A.* **100**: 3584-3588.
4. Ma, L., Kaserer, W., Annamalai, R., Scott, D.C., Jin, B., Jiang, X., Xiao, Q., Maymani, H., Massis, L.M., *et al.* (2007) Evidence of ball-and-chain transport of ferric enterobactin through FepA. *J Biol Chem.* **282**: 397-406.
5. Crosa, J.H. and Walsh, C.T. (2002) Genetics and assembly line enzymology of siderophore biosynthesis in bacteria. *Microbiology and Molecular Biology Reviews.* **66**: 223-249.
6. Leduc, D., Battesti, A. and Bouveret, E. (2007) The hotdog thioesterase EntH (YbdB) plays a role in vivo in optimal enterobactin biosynthesis by interacting with the ArCP domain of EntB. *J. Bacteriol.* **189**: 7112-7126.

7. Lambalot, R.H., Gehring, A.M., Flugel, R.S., Zuber, P., LaCelle, M., Marahiel, M.A., Reid, R., Khosla, C. and Walsh, C.T. (1996) A new enzyme superfamily - the phosphopantetheinyl transferases. *Chem Biol.* **3**: 923-936.
8. Drake, E.J., Nicolai, D.A. and Gulick, A.M. (2006) Structure of the EntB multidomain nonribosomal peptide synthetase and functional analysis of its interaction with the EntE adenylation domain. *Chem Biol.* **13**: 409-419.
9. Lai, J.R., Fischbach, M.A., Liu, D.R. and Walsh, C.T. (2006) Localized protein interaction surfaces on the EntB carrier protein revealed by combinatorial mutagenesis and selection. *J Am Chem Soc.* **128**: 11002-11003.
10. Lai, J.R., Fischbach, M.A., Liu, D.R. and Walsh, C.T. (2006) A protein interaction surface in nonribosomal peptide synthesis mapped by combinatorial mutagenesis and selection. *Proc Natl Acad Sci U S A.* **103**: 5314-5319.
11. Khalil, S. and Pawelek, P.D. (2009) Ligand-induced conformational rearrangements promote interaction between the *Escherichia coli* enterobactin biosynthetic proteins EntE and EntB. *J Mol Biol.* **393**: 658-671.
12. Khalil, S. and Pawelek, P.D. (2011) Enzymatic adenylation of 2,3-dihydroxybenzoate is enhanced by a protein-protein interaction between *Escherichia coli* 2,3-dihydro-2,3-

dihydroxybenzoate dehydrogenase (EntA) and 2,3-dihydroxybenzoate-AMP ligase (EntE). *Biochemistry*. **50**: 533-545.

13. Imperi, F. and Visca, P. (2013) Subcellular localization of the pyoverdine biogenesis machinery of *Pseudomonas aeruginosa*: a membrane-associated "siderosome". *FEBS Lett.* **587**: 3387-3391.

14. Gasser, V., Guillon, L., Cunrath, O. and Schalk, I.J. (2015) Cellular organization of siderophore biosynthesis in *Pseudomonas aeruginosa*: Evidence for siderosomes. *J. Inorg. Biochem.* **148**: 27-34.

15. Kitagawa, M., Ara, T., Arifuzzaman, M., Ioka-Nakamichi, T., Inamoto, E., Toyonaga, H. and Mori, H. (2005) Complete set of ORF clones of *Escherichia coli* ASKA library (a complete set of *E. coli* K-12 ORF archive): unique resources for biological research. *DNA Res.* **12**: 291-299.

16. Datsenko, K.A. and Wanner, B.L. (2000) One-step inactivation of chromosomal genes in *Escherichia coli* K-12 using PCR products. *Proc Natl Acad Sci U S A.* **97**: 6640-6645.

17. Baba, T., Ara, T., Hasegawa, M., Takai, Y., Okumura, Y., Baba, M., Datsenko, K.A., Tomita, M., Wanner, B.L. and Mori, H. (2006) Construction of *Escherichia coli* K-12 in-frame, single-gene knockout mutants: the Keio collection. *Mol Syst Biol.* **2**: 2006.0008.

18. Green, M.R. and Sambrook, J. (2012) *Molecular cloning: a laboratory manual*. Cold Spring Harbor Laboratory Press New York.
19. Payne, S.M. (1994) Detection, isolation, and characterization of siderophores. *Methods Enzymol.* **235**: 329-344.
20. Schwyn, B. and Neilands, J.B. (1987) Universal chemical assay for the detection and determination of siderophores. *Anal Biochem.* **160**: 47-56.
21. Battesti, A. and Bouveret, E. (2012) The bacterial two-hybrid system based on adenylate cyclase reconstitution in *Escherichia coli*. *Methods.* **58**: 325-334.
22. Miller, J.H. (1992) *A short course in bacterial genetics : a laboratory manual and handbook for Escherichia coli and related bacteria*. Cold Spring Harbor Laboratory Press, Plainview, N.Y.
23. Karimova, G., Pidoux, J., Ullmann, A. and Ladant, D. (1998) A bacterial two-hybrid system based on a reconstituted signal transduction pathway. *Proc Natl Acad Sci U S A.* **95**: 5752-5756.
24. Torchala, M., Moal, I.H., Chaleil, R.A., Fernandez-Recio, J. and Bates, P.A. (2013) SwarmDock: a server for flexible protein-protein docking. *Bioinformatics* **29**: 807-809.

25. Sundlov, J.A., Shi, C., Wilson, D.J., Aldrich, C.C. and Gulick, A.M. (2012) Structural and functional investigation of the intermolecular interaction between NRPS adenylation and carrier protein domains. *Chem Biol.* **19**: 188-198.
26. Sundlov, J.A., Garringer, J.A., Carney, J.M., Reger, A.S., Drake, E.J., Duax, W.L. and Gulick, A.M. (2006) Determination of the crystal structure of EntA, a 2,3-dihydro-2,3-dihydroxybenzoic acid dehydrogenase from *Escherichia coli*. *Acta Crystallogr D Biol Crystallogr.* **62**: 734-740.
27. Mattaini, K.R., Brignole, E.J., Kini, M., Davidson, S.M., Fiske, B.P., Drennan, C.L. and Vander Heiden, M.G. (2015) An epitope tag alters phosphoglycerate dehydrogenase structure and impairs ability to support cell proliferation. *Cancer. Metab.* **3**: 5.
28. Magalon, A., Frixon, C., Pommier, J., Giordano, G. and Blasco, F. (2002) *In vivo* interactions between gene products involved in the final stages of molybdenum cofactor biosynthesis in *Escherichia coli*. *J. Biol. Chem.* **277**: 48199-48204.
29. Reznikoff, W.S. (1992) The lactose operon-controlling elements: a complex paradigm. *Mol. Microbiol.* **6**: 2419-2422.
30. Sawma, P., Roth, L., Blanchard, C., Bagnard, D., Crémel, G., Bouveret, E., Duneau, J.-P., Sturgis, J.N. and Hubert, P. (2014) Evidence for new homotypic and heterotypic interactions between transmembrane helices of proteins involved in receptor tyrosine kinase and neuropilin signaling. *J. Mol. Biol.* **426**: 4099-4111.

31. Lensink, M.F., Wodak, S.J. (2013) Docking, scoring, and affinity prediction in CAPRI. *Proteins* **81**: 2082-2095.

32. Comeau, S.R., Gatchell, D.W., Vajda, S., Camacho, C.J. (2004) ClusPro: an automated docking and discrimination method for the prediction of protein complexes. *Bioinformatics* **20**: 45-50.

33. Bonvin, A.M. (2006) Flexible protein-protein docking. *Curr. Opin. Struct. Biol.* **16**: 194-200.

Table 1. PCR primer sequences used for preparing BACTH constructs.

Vector	Gene	Primer Sequence (5'-3')
pUT18C, pKT25	<i>entA</i>	F: TAGGGGTACCTATGGATTTCAGCGGTAAAAATGTCTGGG
		R: CTACGGAATTCTTATGCCCCAGCGTTGAGCC
	<i>entE</i>	F: TAGGGGTACCTATGAGCATTCCATTCACCCGCTGGC
		R: CTACGGAATTCTCAGGCTGATGCGCGTGACG
pUT18, pKNT25	<i>entA</i>	F: TAGGGGTACCTGATTTCAGCGGTAAAAATGTCTG
		R: CTACGGAATTCGACGCATAATCCGGCACATCATACGGATATGCC CCCAGCGTTGAG
	<i>entE</i>	F: TAGGGGTACCTAGCATTCCATTCACCCGCTG
		R: CTACGGAATTCGACGCATAATCCGGCACATCATACGGATAGGCT GATGCGCGTGAC

F = forward, R = reverse. Underlined sequences indicate *KpnI* (forward) and *EcoRI* (reverse) restriction sites. Double underline indicates HA tag.

Table 2. BACTH Constructs: Summary of CAS Assays and Growth Studies.

Vector	Reporter Fragment	Reporter Position	EntA	EntE
pUT18C	T18	N-terminal	+	+
pUT18	T18	C-terminal	-	+
pKT25	T25	N-terminal	+	+
pKNT25	T25	C-terminal	-	+

Figure Legends

Figure 1: Intracellular functionality of BACTH constructs determined by CAS assays and growth studies. Images to the left are photographs of CAS agar plates spotted with various *E. coli* strains and transformants. Enterobactin secretion is indicated by orange halos. Graphs to the right show growth studies of corresponding strains and transformants. All growth studies were performed in iron-depleted minimal medium. Orange bars indicate strains/transformants that exhibited a positive CAS signal; error bars represent standard deviations from mean values ($n=3$). See Results & Discussion section 3.1 for details on all strains and transformants. (A) Untransformed *E. coli* strains. (B) *E. coli* knockout strains transformed with expression constructs harboring hexahistidine-tagged EntA (upper panel) and EntE (lower panel). (C) *E. coli entA* cells transformed with BACTH constructs expressing EntA with N-terminal fusions (T25-EntA and T18-EntA) and C-terminal fusions (EntA-T25 and EntA-T18). (D) *E. coli entE* cells transformed with BACTH constructs expressing EntE with N-terminal fusions (T25-EntE and T18-EntE) and C-terminal fusions (EntE-T25 and EntE-T18). For parts A,C and D, growth assays from left to right correspond to the order of strains/transformants shown in the corresponding CAS assays. For part B, growth assays 1 and 2 correspond to the CAS assays shown in the upper panel. Growth assays 3 and 4 correspond to the CAS assays shown in the lower panel.

Figure 2: Three-dimensional X-ray crystallographic structures of EntA and EntE.

(A) Crystallographic structure of EntA tetramer (PDB code: 2FWM) [26]. (B) Crystallographic structure of EntE monomer taken from the crystallographic structure of the EntB-EntE chimeric

protein (PDB code: 3RG2) [25]. Both proteins are shown as biological assemblies. Chains are colored from N-terminus (blue) to C-terminus (red). Positions of N- and C-termini are indicated.

Figure 3: BACTH assays of the EntA-EntE interaction.

BACTH constructs encoding EntA or EntE fused N- or C-terminally to T25 or T18 were co-transformed into *E. coli* BTH101 cells and assessed for two-hybrid signals. Plasmids used for BACTH constructs were: pKT25 (T25 (N)), pUT18C (T18 (N)), pKNT25 (T25 (C)), and pUT18 (T18 (C)). (A) *E. coli* BTH101 co-transformants spotted onto MacConkey agar. Red colonies are indicative of a positive two-hybrid signal. Left to right: BTH101 co-transformed with pKT25-*entA* and pUT18C-*entE*; BTH101 co-transformed with pUT18C-*entA* and pKT25-*entE*; BTH101 co-transformed with pUT18C-*entA* and pKNT25-*entE*; BTH101 co-transformed with pKT25-*entA* and pUT18-*entE*. (B) Bar graph showing β -galactosidase assays of BACTH co-transformants in (A), as well as relevant empty vector controls ('vec'). An additional control assay in which pKT25-*entA* was co-transformed with pUT18C-*mobA* is also shown. Error bars represent standard deviations from mean values ($n=3$).

Figure 4: Verification of protein expression from BACTH constructs by Western blotting.

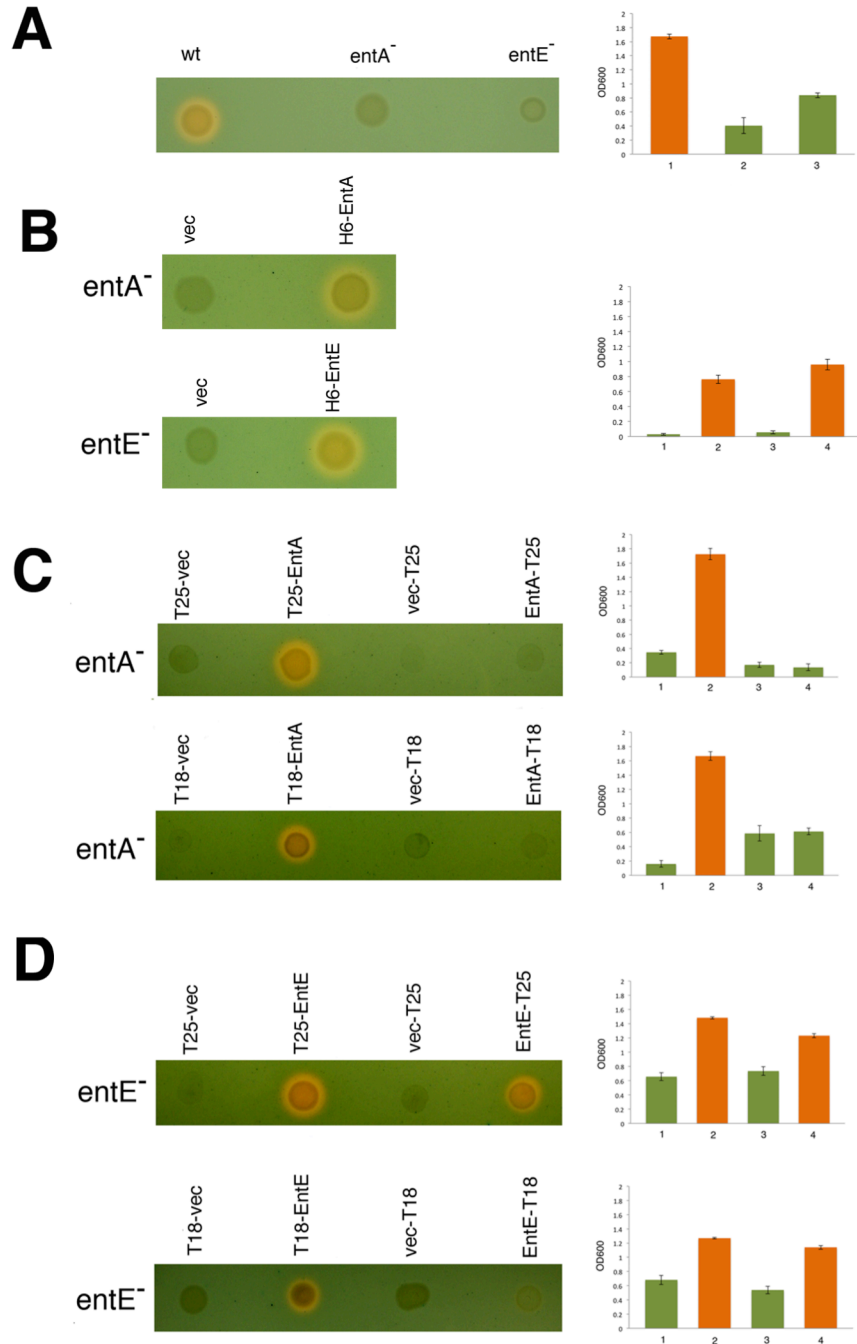
Western blot analysis of protein expression from *entA* and *entE* BACTH constructs. Whole-cell lysates from IPTG-induced *E. coli* BW25113 transformants (equivalent wet cell weights) were analyzed by Western blotting using antibodies against polypeptide fusions as follows: T18 fragments were detected using anti-T18 monoclonal antibody (3D1); T25 fragments were detected by an anti-T25 polyclonal antibody (bN-13); C-terminally tagged T18 and T25

constructs containing an HA tag as a linker were also detected using an anti-HA monoclonal antibody. HRP-conjugated secondary antibodies were detected by chemiluminescence imaging.

Figure 5. Automated docking of monomeric EntE to tetrameric EntA.

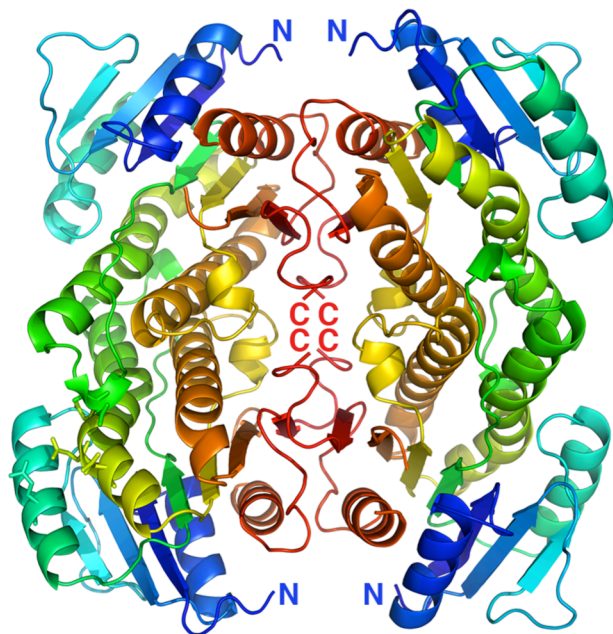
(A) Highest-scoring SwarmDock model showing interaction of EntE monomer (coils, colored from N-terminus (blue) to C-terminus (red)) binding to EntA tetramer (spheres; chains A&D: light grey, chains C&B: dark grey; spheres corresponding to N-terminal atoms of chains C&D are shown as light blue spheres). N-termini of proteins are labeled as follows: N_E : N-terminus of EntE; N_{A_C} : N-terminus of EntA C chain; N_{A_D} : N-terminus of EntA D chain. (B) EntE-EntA interaction interface. Proteins in the SwarmDock-predicted complex were computationally separated by rotating EntE (left: yellow surface) by 180° and then translating it in the x-axis relative to EntA tetramer (right: chain A: blue surface, chain B: red surface, chain C: pink surface, chain D: light blue surface). EntE residues within 4 Å of EntA are colored according to EntA subunit. EntA residues within 4 Å of EntE are colored yellow.

Pakarian & Pawelek, Figure 1

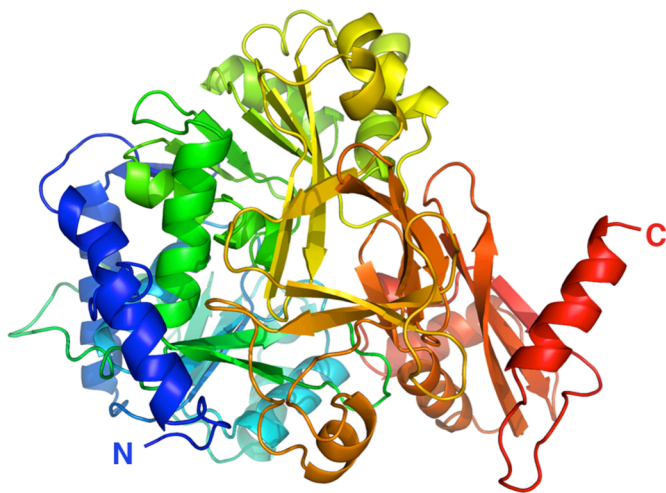


Pakarian & Pawelek, Figure 2.

A



B



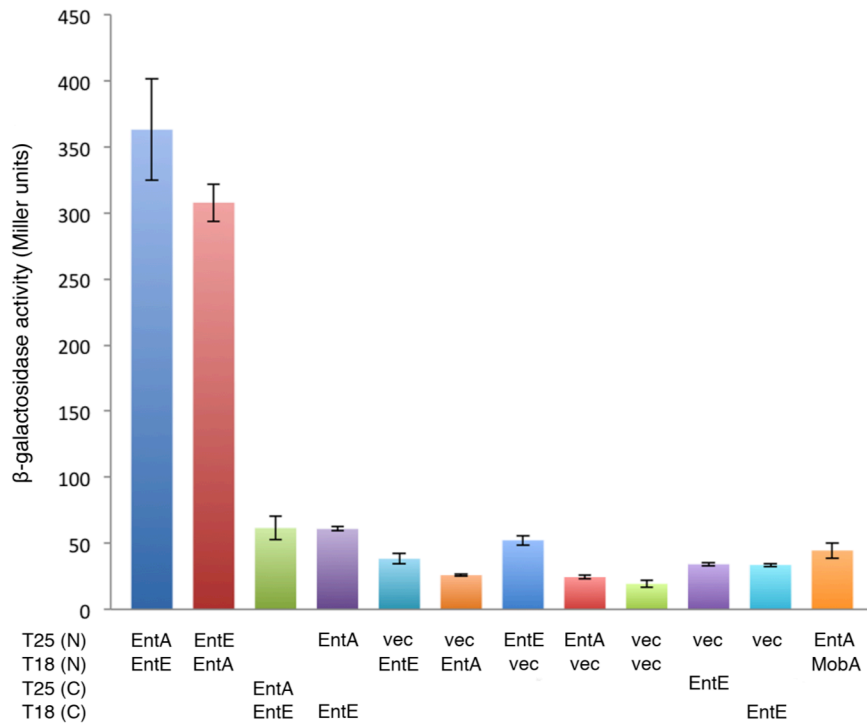
Pakarian & Pawelek, Figure 3.

A















T25 (N)	EntA	EntE		EntA
T18 (N)	EntE	EntA	EntA	
T25 (C)			EntE	
T18 (C)				EntE

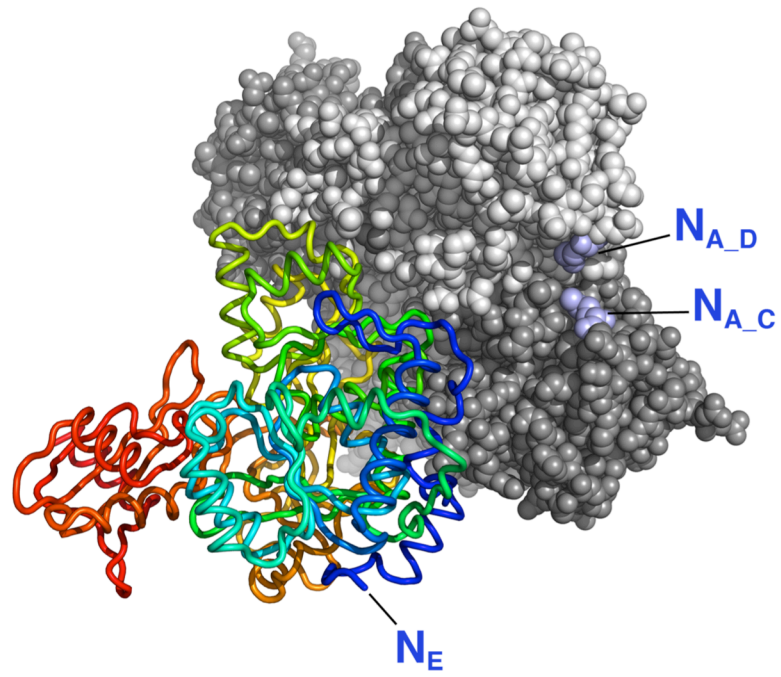
B



Pakarian & Pawelek, Figure 4.

Vector	Reporter Fragment	HA Tag	Primary Antibody	EntA	EntE
pUT18C	N-terminal T18	-	3D1		
pUT18	C-terminal T18	✓	3D1		
			HA		
pKT25	N-terminal T25	-	bN-13		
pKNT25	C-terminal T25	✓	bN-13		
			HA		

A



B

